Real-Time Monitoring of Aluminum Oxidation Through Wide Band Gap MgF_2 Layers for Protection of Space Mirrors

Brian I. Johnson,[a] Tahereh Gholian Avval,[a] Grant Hodges,[a] Karen Membreno,[a] David D. Allred,[b] Matthew R. Linford[a]

[a]Department of Chemistry and Biochemistry, Brigham Young University, C100 BNSN, Provo, Utah 84602
[b]Department of Physics and Astronomy, Brigham Young University, N265 ESC, Provo, Utah 84602

Abstract

Because of its extraordinary and broad reflectivity, aluminum is the only logical candidate for advanced space mirrors that operate deep into the UV. However, aluminum oxidizes rapidly in the air, and even a small amount of oxide (as little as a nanometer) can have a noticeable, detrimental impact on its reflectivity at short wavelengths. Thin films of wide band gap materials like MgF_2 have previously been used to protect aluminum surfaces. Here we report the first real-time, spectroscopic ellipsometry (SE) study of aluminum oxidation as a function of MgF_2 over layer thickness, which ranged from 0 – 6 nm. SE data analysis was performed vis-à-vis a multilayer optical model that included a thick silicon nitride layer. The optical constants for evaporated aluminum were initially determined using a multi-sample analysis (MSA) of SE data from MgF_2 protected and bare Al surfaces. Two models were then considered for analyzing the real-time data obtained from Al/MgF_2 stacks. The first used the optical constants of aluminum obtained in the MSA with two adjustable parameters: the thicknesses of the aluminum and aluminum oxide layers. The thicknesses obtained from this model showed the expected trends (increasing Al_2O_3 layer thickness and decreasing Al layer thickness with time), but some of the Al_2O_3 thicknesses were unphysical (negative). Because the optical constants of very thin metals films depend strongly on their structures and deposition conditions, a second, more advanced model was employed that fit the optical constants for Al, and also the Al and Al_2O_3 thicknesses, for each data set. In particular, the Al and Al_2O_3 thicknesses and optical constants of Al were determined in an MSA for each of 50 evenly spaced analyses in each four-hour dynamic run performed. The resulting optical constants for Al were then fixed for that sample and the thicknesses of the Al and Al_2O_3 layers were determined. While the first and second models yielded similar Al and Al_2O_3 thickness vs. time trends, the film thicknesses obtained in this manner were more physically reasonable. Thicker MgF_2 layers slow the oxidation rate of aluminum. The results from this work should prove useful in protecting space mirrors prior to launch.

1. Introduction

Aluminum is a plentiful, inexpensive metal with a myriad of applications.[1-3] One of these is as a reflector for astronomical observation. Indeed, aluminum is the best-suited reflective coating for space mirrors because of its unmatched ability to reflect over a wide energy range, including into the deep UV.[4, 5] However, a significant challenge in working with aluminum is the speed with which its surface oxidizes in the air.[5-7] The resulting oxide absorbs short wavelength light, which limits aluminum's performance.[5, 8] To overcome this deficiency, wide band gap, protective coatings, e.g., MgF_2, have been deposited onto aluminum mirrors.[9, 10] This approach was taken with the Hubble space telescope. That is, the goal of depositing thin, fluoride-based, inorganic layers onto aluminum mirrors is to create a robust layer that prevents (or limits) oxidation of aluminum prior to launch while allowing adequate reflection at lower wavelengths.[4, 5, 9, 11] In order to maintain satisfactory reflectance at shorter wavelengths, inorganic fluoride barrier layers can only be ca. 3 nm thick, which still allows significant oxygen leakage. Accordingly, a number of studies have focused on developing robust, transparent passivation layers for aluminum.[5, 11]

For this study, we prepared and studied 0 – 6 nm protective coatings of MgF_2 on Al using real-time/dynamic spectroscopic ellipsometry (SE). Both the Al and MgF_2 were deposited by thermal evaporation. The resulting optical stacks were analyzed in real-time with SE scans taken repeatedly over four hours. The optical constants of extremely thin metal films can vary greatly depending on thickness, morphology, and deposition conditions. Accordingly, the optical constants of aluminum evaporated with our deposition system of the approximate thickness used in our study were obtained from a multi-sample analysis (MSA) of aluminum films coated with thick MgF_2 layers and bare, but oxide-coated, aluminum. A relatively simple model with two parameters (the thicknesses of the aluminum and aluminum oxide layers) was then applied to the dynamic data obtained from each sample. The trends (rates of oxidation of aluminum) obtained in this study were reasonable. As expected, thicker MgF_2 films led to slower oxidation of the underlying aluminum. However, some of the thicknesses of the Al_2O_3 films in this modeling were unphysical – they were negative. Accordingly, a second model was applied to the data in which the parameters that governed the aluminum optical constants were varied along with the thicknesses of the aluminum and alumina layers. This model yielded essentially the same rate constants for aluminum oxidation, but more physically satisfying Al_2O_3 thicknesses.

2. Experimental

2.1 Deposition of Al and MgF_2

Thin films of aluminum were deposited with a Denton DV-502 A thermal evaporator. This tool employs two independent resistance-heated sources and a rotating stage. The film thickness was measured and controlled in situ during the deposition using an Inficon quartz crystal monitor (QCM). For depositions, a piece of high purity aluminum wire, 1" long, was placed into a tungsten resistance heater coil, and ca. 15 g of MgF_2 was placed into a molybdenum boat. After the evaporator reached a base pressure of 4 x 10^{-6} Torr, the Al heater was turned on to achieve a deposition rate of 35 Å/s. After 150 Å of Al was deposited, the QCM automatically closed the shutter between the deposition source and the substrate, and MgF_2 was immediately deposited at a rate of 3 Å/s. The overall deposition of both Al and MgF_2 took 35 – 45 s. The substrate was not heated for these depositions – the sample was nominally at room temperature. Directly following the depositions of Al and MgF_2, the chamber was vented with N_2 gas, which took 1.5 – 2.0 min. The samples were then removed and rushed to the SE and XPS instruments for measurement. These transfers took approximately 5 min. The time from sample removal from the chamber to analysis was recorded.

2.2 Instrumentation

SE was performed with a variable angle spectroscopic ellipsometer (M-2000D, J.A. Woollam Company, Lincoln, ME, USA, wavelength range: ca. 190-1688 nm). Series of time-dependent SE measurements were obtained using the 'in situ' mode of the instrument, which allowed the ellipsometer to acquire SE data from a sample every 2.3 s over a period of 4 h. Data were acquired at 75° and subsequently modelled using the CompleteEASE® SE instrument analysis software. The model in Figure 1, which shows the types of stacks prepared and studied in this work, employed optical constants that were obtained as follows. The 'Si Substrate' layer was modeled with the optical constants for silicon in the instrument software, and 'Layer 1 – SiO_2' and 'Layer 3 – SiO_2' were modeled with the optical constants for silicon native oxide in the instrument software. The optical constants for 'Layer 2 – Si_3N_3' were obtained by reformulating/reparameterizing the optical constants for silicon nitride in the instrument software as a Tauc-Lorentz and a Gaussian oscillator. The optical constants for 'Layer 4 – Al' were obtained from a

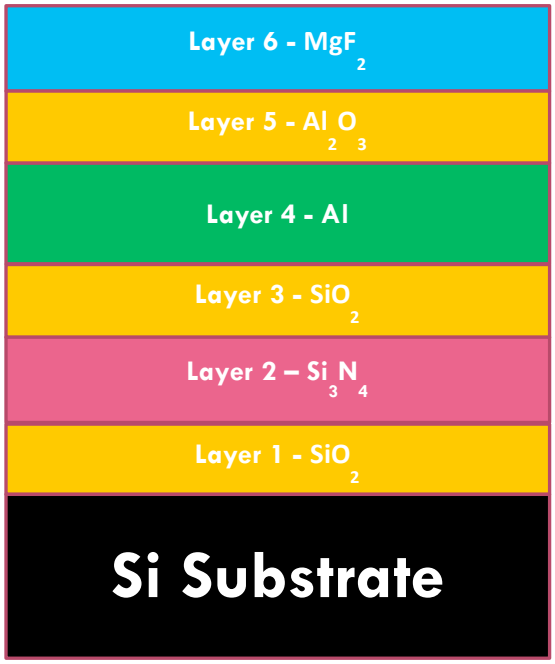

Figure 1. Representation of the optical stacks prepared and analyzed in this work. The bottom layers up through Layer 3 represent the Si/Si_3N_4 substrate. Layers 4 and 6 represent the Al and Mg deposited on the substrate. Layer 5 represents the oxidized Al that forms on the Al layer.

multi-sample analysis as described below. The 'Layer 5 – Al_2O_3' and 'Layer 6 – MgF_2' layers were modeled with the optical constants for these materials in the instrument software. XPS was performed using an SSX-100 instrument with a hemispherical analyzer (maintained by Service Physics, Bend, OR, USA). The instrument employed monochromatic Al Kα X-rays and had a take-off angle of 35°. Survey scans were obtained with a spot size of 800 x 800 μm^2 with a resolution of 4 (nominal pass energy of 150 eV). Each survey spectrum is the average of 6 scans (passes) with a step size of 1 eV. In general, high-resolution (narrow) scans had a window width of 40 eV and a step size of 0.0625 eV. The spot size was again 800 x 800 μm^2, the resolution was 4 (nominal pass energy of 150 eV), and 20 scans were averaged to obtain each spectrum. Peak fitting was performed with CasaXPS (Casa Software Ltd., Version 2.3.18PR1.0).

3. Results and Discussion

In spectroscopic ellipsometry (SE), light of a known polarization state is directed onto a surface, and changes in that polarization are detected. Through creation of models and adjustment of the parameters in them, SE can be used to determine a variety of material properties including film thicknesses, surface roughness, and optical constants of materials. However, due to the complexity of the optical stack in the present work (see Figure 1), the thicknesses of the MgF_2 and Al_2O_3 layers, as determined by SE, appeared to be correlated. Accordingly, the thickness of the MgF_2 layer in each optical stack was determined separately by XPS, which was then fixed to this value in the subsequent SE modeling. The following procedure describes how these measurements and calculations were performed.

1. Different thicknesses of MgF_2, which covered the range of thicknesses of interest in this study, were deposited onto shards of native oxide-terminated silicon (Si/SiO_2). Prior to these depositions, the thicknesses of the native oxide layers were determined by SE using the optical constants for native oxide and crystalline silicon in the instrument software.
2. The thicknesses of the MgF_2 thin films were determined by SE using the optical constants of MgF_2 in the instrument software with the thicknesses of the SiO_2 layers fixed to those obtained for each shard prior to the MgF_2 depositions.
3. These same samples ($Si/SiO_2/MgF_2$) were then analyzed by XPS, and the areas of the Mg 2s and Si 2p peaks (all chemical states) were determined using CasaXPS. These areas were then inserted into Equation 1 [12, 13]

$$\ln\frac{(I_o/s_o)}{(I_s/s_s)} - \left[\left(\frac{E_o}{E_s}\right)^{0.75} - \frac{1}{2}\right]\frac{t}{\lambda_o \cos\theta} - \ln 2 = \ln sinh\left(\frac{t}{\lambda_o \cos\theta}\right) \quad (1)$$

Here, I_o and s_o are the intensity and sensitivity factor respectively of the MgF_2 layer, and I_s and s_s are the intensity and sensitivity factor of the substrate (Si). These sensitivity factors (s_o and s_s) were obtained from CasaXPS. E_o and E_s are the binding energies of the Mg 2s and Si 2p signals, respectively, and λ_o is the attenuation length of the Mg 2s photoelectrons in MgF_2. With this information, the value of λ_o was the only unknown in

Equation 1. The value of λ_o was then adjusted until the two sides of Equation 1 were equal. This approach was taken with four thicknesses of MgF_2 that yielded four λ_o values, as follows: (1.6 nm MgF_2, λ_o: 6.1 nm), (2.1 nm MgF_2, λ_o: 5.3 nm), (3.3 nm MgF_2, λ_o: 4.6 nm), and (5.1 nm MgF_2, λ_o: 4.2 nm). This limited set of data suggests that as the MgF_2 film thickness increases, the attenuation length through it decreases. This would be consistent with the deposition of an increasingly dense film of MgF_2 as its thickness increases, i.e., the defects in the film may be increasingly filled in as it becomes thicker. Because most of the MgF_2 thicknesses used in this study were more than 2 nm thick, a λ_o value of 4.5 nm was chosen for this work.

4. With a value of λ_o for Mg 2s photoelectrons in MgF_2, Equation 1 was used again, but this time to solve (iteratively again) for the thickness of a MgF_2 layer. In this case, the substrate was considered to be Al, and the entire Al 2p peak area (all chemical states) was employed in the calculations. That is, XPS was performed on each optical stack to obtain the intensities of the Mg 2s and Al 2p peaks that were needed for Equation 1.
5. The results obtained from this method were within about 5% of the values predicted during each deposition by the QCM, where the QCM had previously been calibrated with MgF_2 thicknesses obtained from this material on native oxide-terminated silicon shards.

Overall, this approach should account for any run-to-run variation in the deposition of the MgF_2.

The optical constants of thin metal films depend strongly on their structure and deposition conditions.[14, 15] Thus, it was necessary to determine the optical constants of the Al films produced with our evaporation system, i.e., while those in the instrument software might an appropriate starting point, it is unlikely they would be suitable for our modeling. The determination of the optical constants of aluminum was done using an MSA with (i) three Al films (nominally 15 nm thick) that were covered with thick films of MgF_2 (nominally 25 nm thick) and (ii) one bare aluminum surface (nominally 15 nm thick). These layers were deposited onto silicon nitride ($Si/SiO_2/Si_3N_4/SiO_2$) substrates (the nominal thicknesses of the Si_3N_4 layers in these stacks was 300 nm). The bare aluminum film was expected to have some oxide on it, i.e., it was modeled as an aluminum layer beneath an Al_2O_3 layer. For this modeling, the optical constants of Al_2O_3 from the instrument software were used. Because of the thicknesses of the MgF_2 layers here, it was assumed that they had no aluminum oxide under them. Note that the MgF_2 thickness could be determined directly by SE here because no Al_2O_3 was present. The starting point for the optical constants of Al in these analyses was the "Al (Lorentz).mat" model in our instrument software, which contains seven Lorentzian oscillators. To determine the optical constants for our evaporated aluminum, the amplitudes and breadths, but not the positions, of these Lorentzians were allowed to vary one at a time. In this analysis, the amplitude of one of the Lorentzians went to zero so it was omitted. Prior to the deposition of Al and MgF_2, the thicknesses of the layers in the substrate (from the 'Si Substrate' through 'Layer 3 – SiO_2' layer) were measured, modeled, determined, and then fixed.

To study the MgF_2 passivation of aluminum, Al (nominal thickness of 15 nm) and then MgF_2 (different thicknesses) were deposited onto fully characterized $Si/SiO_2/Si_3N_4/SiO_2$ substrates.

These $Si/SiO_2/Si_3N_4/SiO_2/Al/MgF_2$ stacks were then removed from the evaporation chamber, which 'started the clock' for the sample. As quickly as possible, each sample was moved to the ellipsometer, and a four-hour run was commenced that repeatedly collected SE data from the sample. The stack was then analyzed by XPS to determine the thickness of its MgF_2 layer. Two models were finally used to analyze each four-hour set of SE data.

MgF_2 Thickness	Model 1 MSE	Model 2 MSE
0.000 nm	1.20	0.31
1.726 nm	0.75	0.41
2.096 nm	15.49	1.39
2.847 nm	3.28	2.93
3.550 nm	300.00	7.62
3.554 nm	1.23	0.37
4.322 nm	0.75	0.31
4.544 nm	16.96	3.51
5.358 nm	0.83	0.25
5.974 nm	33.69	5.81
Samples w/neg. Al_2O_3 thicknesses	6 of 9	2 of 10
Samples that could not be fit	1	0

Table 1. Results from the two models used to analyze the dynamic sets of SE data generated in this study.

The first SE model (Model 1) was based on (i) previous characterization of the $Si/SiO_2/Si_3N_4/SiO_2$ substrates with all layer thicknesses and optical constants fixed, (ii) the optical constants that had been generated for a ca. 15 nm Al film in the four-sample MSA described above, (iii) the optical constants of Al_2O_3 that were in the instrument software, and (iv) the thickness of MgF_2 that had been determined by XPS and the optical constants of MgF_2 from the instrument software. Thus, there were only two unknowns in Model 1, which were the thicknesses of the Al and Al_2O_3 films (see again Figure 1). This model was applied to each set of dynamic data collected in each four-hour analysis from 10 samples with different MgF_2 thicknesses. Table 1 presents the mean squared error (MSE) value of the fits obtained with Model 1 for each of these samples. It is clear here that some of the data sets are well fit (lower MSE values), while others are poorly fit (higher MSE values). Table 1 also reports that with Model 1, one of the samples could not be fit (the one with an MSE of 300), and 6 of the remaining 9 samples showed at least some Al_2O_3 thicknesses that were negative, which is obviously unphysical. Figure 2 shows representative results from Model 1 for two samples with different MgF_2 thicknesses that gave positive and negative thicknesses for the Al_2O_3 layer.

In spite of the fact that Model 1 predicted negative Al_2O_3 thicknesses for a significant fraction of the samples, all of the Al_2O_3 and Al thicknesses for the samples that could be fit showed the same trends, which were increasing Al_2O_3 thicknesses and decreasing Al thicknesses. Indeed, it was found that the plots of the Al_2O_3 thicknesses vs. the log of time for the different samples yielded, approximately, straight lines, and that they could be reasonably fit to an equation of the form:

$$(2) \qquad t_{Al2O3} = k \ln t + b$$

where t_{Al2O3} is the thickness of the Al_2O_3 film, t is time, k represents the rate of oxidation of the sample, and b is the y-intercept of the line. Figure 3 shows the values of k that were thus obtained as a function of the MgF_2 thickness of the samples. It is clear that k decreases as the thickness of the MgF_2 over layer increases, which is the expected behavior for this system.

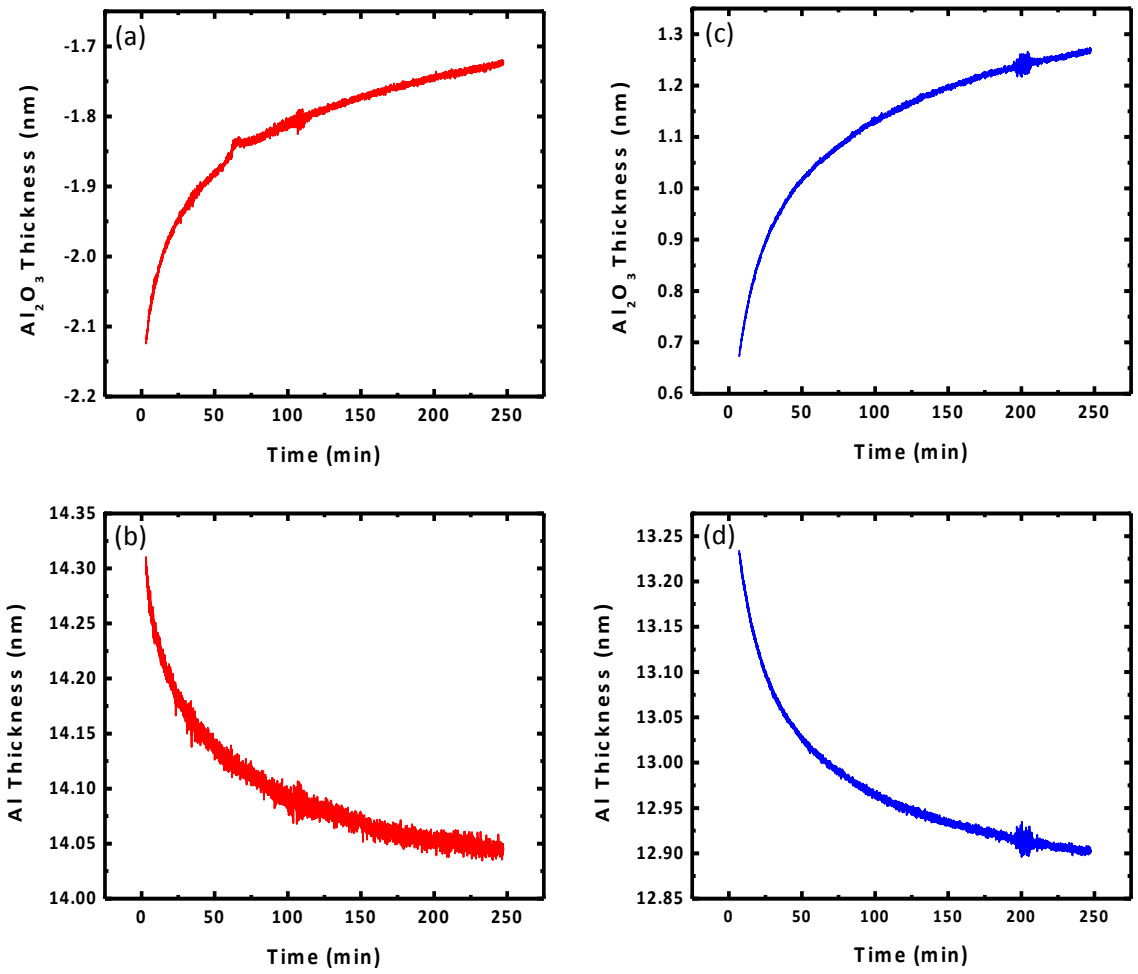

Figure 2. Thicknesses of Al_2O_3 and Al determined by Model 1 from two representative samples that showed negative (a) and positive (c) Al_2O_3 thicknesses. Also shown are the Al thicknesses obtained as a function of time for these surfaces.

The negative thicknesses for Al_2O_3 predicted by Model 1 are somewhat disconcerting. We reasoned that perhaps this model was giving unphysical results for this layer because we were requiring the same Al optical constants to be applied to all the stacks – we previously noted that optical constants for extremely thin metal films are *not* constant. Accordingly, a second SE model/approach (Model 2) was developed in which the optical constants of Al were determined/allowed to vary for each sample, i.e., the amplitudes and breadths, but not the center energies, of all the Lorentzians varied. The thicknesses of the Al and Al_2O_3 layers also varied in this model. The lower MSE values for Model 2 (see Table 1) suggested that this approach more closely represented each material. In other words, these improved MSE values support the idea that the Al optical constants vary between the samples. Two other indications that Model 2 is an improved representation of our materials are that all of the samples could be fit with Model 2, and that only 2 of the 10 samples showed negative Al_2O_3 thicknesses. Plots of Al_2O_3 thickness vs. the log of time were again found to be quite linear and were fit with Equation 2. The resulting k values are plotted in Figure 4. It is significant that they are nearly identical to those obtained with Model 1. That is, these results suggest that the decrease in k observed with increasing MgF_2 thickness is not an artifact of either measurement.

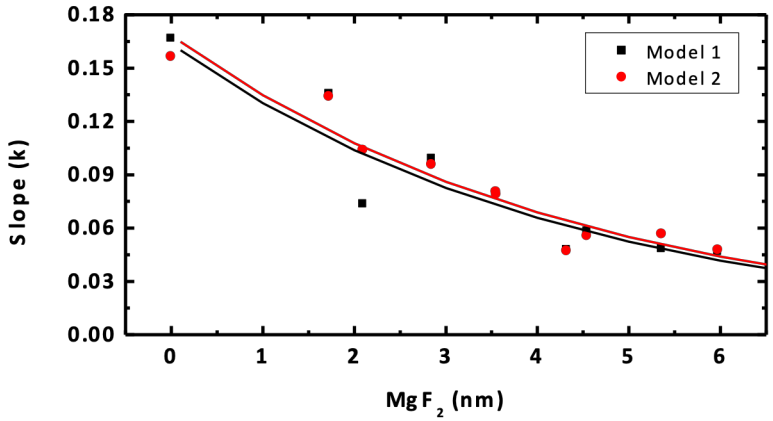

Figure 3. Values of k determined from Equation 1 from data generated from Models 1 and 2 employed in this study.

4. Conclusions

We have shown real time (dynamic) SE analysis of ten MgF_2 - coated aluminum thin films. The MgF_2 thicknesses were determined by a combination of XPS and SE. The optical constants of the Al films were initially estimated via an MSA of similar materials. Two different models were employed to work up the Al_2O_3 thickness vs. time data generated from the dynamic SE analyses. While the second model gave more physically reasonably results, both made nearly identical predictions of the rate constants for Al oxidation beneath MgF_2 coatings. We believe these results will contribute to an understanding of Al mirror oxidation that will help prepare Al mirrors for space.

5. Future Work/Publication

A more complete treatment of these and other results is being written. It will include XPS analysis showing oxidation of aluminum vs. time and more advanced SE modeling.

6. Acknowledgments

The authors gratefully thank and acknowledge the Utah NASA Space Grant Consortium for funding this work.

7. References

1. Skillingberg, M.; Green, J., Aluminum applications in the rail industry. **2007,** *65* (5), 8.
2. Bertram, M.; Martchek, K. J.; Rombach, G. J., Material flow analysis in the aluminum industry. **2009,** *13* (5), 650-654.
3. Das, S.; Yin, W. J., Trends in the global aluminum fabrication industry. **2007,** *59* (2), 83-87.
4. Hass, G.; Tousey, R. J., Reflecting coatings for the extreme ultraviolet. **1959,** *49* (6), 593-602.
5. Bridou, F.; Cuniot-Ponsard, M.; Desvignes, J.-M.; Maksimovic, I.; Lemaire, P. In *VUV mirrors for the (80-120 nm) spectral range*, Advances in Optical Thin Films, International Society for Optics and Photonics: 2004; pp 627-637.
6. Trost, J.; Brune, H.; Wintterlin, J.; Behm, R.; Ertl, G., Interaction of oxygen with Al (111) at elevated temperatures. **1998,** *108* (4), 1740-1747.
7. Brune, H.; Wintterlin, J.; Behm, R.; Ertl, G., Surface migration of ''hot''adatoms in the course of dissociative chemisorption of oxygen on Al (111). **1992,** *68* (5), 624.
8. Zhukovskii, Y. F.; Jacobs, P.; Causá, M.; Solids, C., On the mechanism of the interaction between oxygen and close-packed single-crystal aluminum surfaces. **2003,** *64* (8), 1317-1331.
9. Fernández-Perea, M.; Larruquert, J. I.; Aznárez, J. A.; Pons, A.; Méndez, J., Vacuum ultraviolet coatings of Al protected with MgF_2 prepared both by ion-beam sputtering and by evaporation. **2007,** *46* (22), 4871-4878.
10. Wilbrandt, S.; Stenzel, O.; Nakamura, H.; Wulff-Molder, D.; Duparré, A.; Kaiser, N., Protected and enhanced aluminum mirrors for the VUV. **2014,** *53* (4), A125-A130.
11. De Marcos, L. V. R.; Larruquert, J. I.; Méndez, J. A.; Gutiérrez-Luna, N.; Espinosa-Yáñez, L.; Honrado-Benítez, C.; Chavero-Royán, J.; Perea-Abarca, B., Optimization of MgF_2-deposition temperature for far UV Al mirrors. **2018,** *26* (7), 9363-9372.
12. Cumpson, P., Application of techniques for the analysis of surfaces. The thickogram: a method for easy film thickness measurement in XPS. **2000,** *29* (6), 403-406.
13. Cumpson, P. J.; Seah, M. P., Application of techniques for the analysis of surfaces. Elastic scattering corrections in AES and XPS. II. Estimating attenuation lengths and conditions required for their valid use in overlayer/substrate experiments. **1997,** *25* (6), 430-446.
14. Girtan, M.; Rusu, G.; Rusu, G. J. M. S.; B, E., The influence of preparation conditions on the electrical and optical properties of oxidized indium thin films. **2000,** *76* (2), 156-160.
15. Martin, P., Ion-based methods for optical thin film deposition. **1986,** *21* (1), 1-25.